Nucleation and growth of Ag islands on fivefold Al-Pd-Mn quasicrystal surfaces: Dependence of island density on temperature and flux

B. Unal, V. Fournée, K. J. Schnitzenbaumer, C. Ghosh, C. J. Jenks, A. R. Ross, T. A. Lograsso, J. W. Evans, P.A. Thiel

Nucleation and growth of Ag islands on fivefold Al-Pd-Mn quasicrystal surfaces: Dependence of island density on temperature and flux

B. Unal,[1] V. Fournée,[2] K. J. Schnitzenbaumer,[1] C. Ghosh,[1] C. J. Jenks,[1] A. R. Ross,[1] T. A. Lograsso,[1] J. W. Evans,[1] and P. A. Thiel[1]

[1]*Ames Laboratory and Departments of Chemistry, Materials Science and Engineering, and Mathematics, Iowa State University, Ames, Iowa 50011, USA*

[2]*LSG2M, CNRS-UMR7584, Ecole des Mines, Parc de Saurupt, 54042, Nancy, France*

(Received 31 August 2006; revised manuscript received 22 November 2006; published 9 February 2007)

Scanning tunneling microscopy (STM) has been used to investigate the nucleation and growth of Ag islands on the fivefold surface of an icosahedral Al-Pd-Mn quasicrystal. Analysis of the data as a function of deposition temperature, from 127 K to 300 K, reveals that island density is constant, while at higher temperature it decreases. To model this behavior, we first show that the potential energy surface describing bonding of Ag at various locations on the surface is complex, with a few sites acting as traps for clusters of adatoms. We then develop a rate equation model which incorporates enhanced nucleation at trap sites relative to nucleation at regular sites on terraces. It recovers the temperature dependence of the island density, plus previous flux-scaling data. Our model suggests that the critical size for both types of nucleation sites is large—corresponding to stable clusters of at least 6 Ag atoms—and that binding between atoms at trap sites is significantly stronger than at free terrace sites. The data and the model, combined, provide guidance about the conditions of temperature and flux under which saturation of trap sites can be expected. This, in turn, provides a general indicator of the conditions that may favor localized pseudomorphic growth at low coverage, here and in other systems.

DOI: 10.1103/PhysRevB.75.064205 PACS number(s): 61.44.Br, 68.55.Ac, 68.43.Jk

I. INTRODUCTION

Quasicrystals are well ordered but nonperiodic materials.[1] Their atomic structure is associated with interesting surface properties[2,3] such as enhanced oxidation resistance[4] and low friction.[5] In recent years, much attention has been paid to the possibility that films might be grown pseudomorphically on quasicrystal surfaces, thereby yielding surfaces that derive the benefits of the quasiperiodic structure, but with a wider range of chemical composition than is accessible in bulk samples.[6–8] Pseudomorphic growth was indeed demonstrated experimentally, originally by Franke *et al.*,[9] and later by other groups, for certain types of elemental adlayers.[10–12] Pseudomorphic growth has also been explored theoretically.[13,14] The properties of such films remain largely unexplored, but preliminary measurements of their electronic structure suggest that they adopt the pseudogap at the Fermi edge which is associated with the underlying substrate.[15]

Many studies of film growth have focused on coverages of a complete monolayer (ML) or above, since contiguous coatings would be desirable for some applications. However, lower coverages may also be interesting. For example, individual pseudomorphic islands might exhibit peculiar magnetic properties. Pseudomorphism could be more prevalent at submonolayer coverages, where adsorbate-adsorbate interactions are more localized, and distortions from the bulk structure of the film are thus more easily accommodated. This appears to be illustrated by our previous study of Al adsorbed on the fivefold surface of the icosahedral (*i*-) quasicrystal Al-Cu-Fe, where small fivefold clusters were observed at a coverage of about 0.04 ML.[10] In comparison, pseudomorphism was not observed in studies of Al at or above coverages of 1 ML on a similar substrate, *i*-Al-Pd-Mn.[16] Formation of the pseudomorphic clusters in the former case was corroborated theoretically using a kinetic Monte Carlo (KMC) simulation of an appropriate "disordered bond network" lattice gas model.[17]

An equally-important advantage of studying low coverages is that a wealth of information can be extracted about the *kinetics* of island nucleation and growth in the initial stages of film formation. This has been shown by the large body of work on crystalline substrates and films.[18] For this purpose, scanning tunneling microscopy (STM) provides invaluable detailed insight. This is because the spatial characteristics of films at low coverages, such as the island density, reflect the kinetics of nonequilibrium adlayer evolution during deposition. Based upon just such data, we previously found evidence for heterogeneous nucleation of Ag on the fivefold surface of *i*-Al-Pd-Mn at 300 K.[19] We interpreted the observed flux-*in*dependence of island density to mean that nucleation occurred preferentially at specific sites—not defect sites, but rather trap sites intrinsic to the quasicrystalline structure. We speculated that these trap sites were analogous to those that stabilized the pseudomorphic Al starfish on *i*-Al-Cu-Fe.

In this paper, we extend the previous Ag work by measuring the temperature dependence of Ag island density at ~0.2 ML, and by showing the data to be compatible with a refined mean field-rate equation model that incorporates nucleation at trap sites. We delineate the conditions of temperature and flux under which one can expect saturation of trap sites, which provides a general indicator of the conditions that may favor localized pseudomorphic growth at low coverage, in this and other systems.

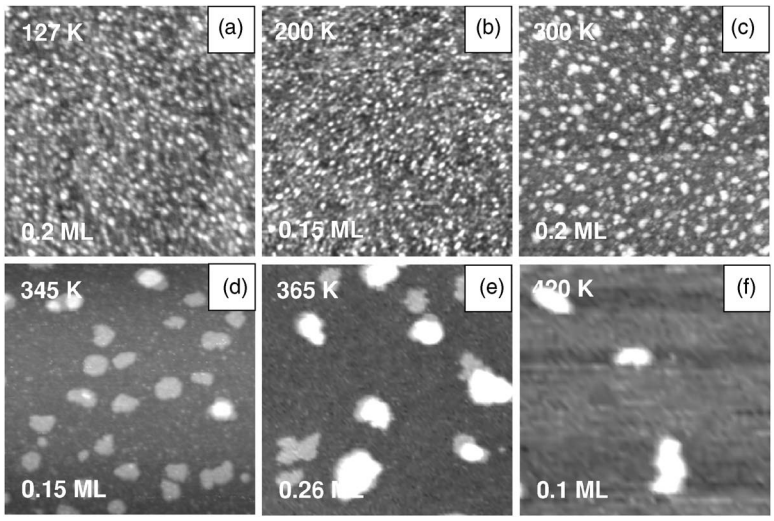

FIG. 1. STM images [(a)-(f)] showing the evolution of island density as a function of temperature for deposition of Ag onto 5*f*-*i*-Al-Pd-Mn quasicrystal. The size of images is 100×100 nm^2. The tunneling conditions are 0.97–0.99 V and 0.31–0.47 nA.

II. EXPERIMENTAL DESCRIPTION

We conduct our experiments using an Omicron variable-temperature STM in a standard UHV chamber with a base pressure of 4×10^{-11} mbar. Our sample is a single grain of icosahedral $Al_{70.2}Pd_{20.7}Mn_{9.1}$ quasicrystal with the surface oriented perpendicular to a fivefold axis. The clean surface is prepared following procedures described elsewhere.[20,21] Ag is deposited from an electron-beam-heated evaporator, an Omicron evaporator with internal flux monitor modified to resemble a Knudsen cell, onto the clean quasicrystal surface at fixed sample temperatures varying from 127 K to 420 K and at chamber pressures below 8×10^{-11} mbar. STM images are taken at the deposition temperature. STM data are processed using image processing freeware.[22]

III. EXPERIMENTAL RESULTS

Figure 1 shows a series of STM images taken after deposition of 0.1 to 0.26 monolayers (ML) of Ag at a constant flux of 1×10^{-3} ML/s and various substrate temperatures. The brighter features in the images are Ag islands. For the temperature range of 127 K to 300 K, island sizes are very small as compared to those at higher temperatures, and the island density is high. A dramatic decrease in the island density and corresponding increase in size is apparent for temperatures above 300 K. At 420 K [Fig. 1(f)], most of the deposited Ag accumulates at step edges (not shown in the image). This indicates that the diffusion length has become comparable to the terrace width. However, particularly broad terraces still support island formation, an example of which is shown in Fig. 1(f). This allows a rough assessment of island density at this temperature.

It should also be noted that, at these low coverages, islands are typically two-dimensional (2D) at $T<300$ K, but three-dimensional (3D) at $T>300$ K. The 3D growth has been ascribed to a quantum size effect.[23] While this crossover from 2D to 3D shapes does not affect our determination and modeling of island densities, it will affect the interpretation of island sizes, as discussed later in this section.

At and below 300 K, the determination of coverage or of island number density is complicated by the fact that the clean surface has a rather high intrinsic corrugation, together with occasional protrusions. In high-resolution images of well-ordered regions of clean terraces, the peak-to-peak corrugation is about 0.12 to 0.16 nm, to be compared with the expected step height for a Ag island of about 0.2 nm. (Note that these values depend somewhat on tunneling bias.) The corrugation and step height are sufficiently close that scanning across Ag islands on the quasicrystal produces a continuum of heights without a clear separation of island and substrate contributions, as shown in Fig. 2 for a coverage of 0.2 ML at 300 K. The large maximum at about 0.1 nm represents the clean substrate, whereas the smaller maximum at about 0.3 nm represents the Ag islands. To determine the island density, we introduce a threshold for height located between these peaks, chosen such that regions with heights above the threshold are mainly associated with Ag islands (see Fig. 2). To further eliminate artifacts in island density estimation due to the existence of occasional protrusions on the quasicrystal surfaces,[24] we employ a threshold for the minimum areal size in addition to the height cutoff. This areal cutoff affects the data only at low temperature, where the Ag islands are small. The effect is shown by the error

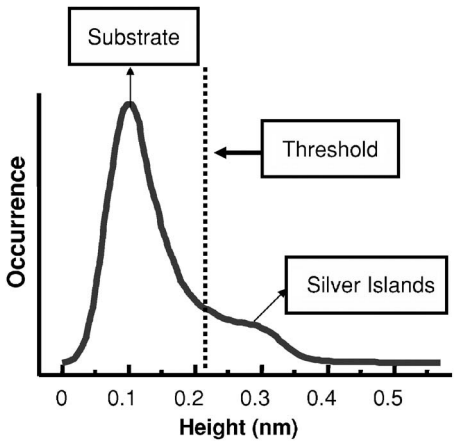

FIG. 2. An area based height histogram taken from an STM image at $\theta=0.2$ ML and $T=300$ K. Dotted line shows the threshold which partially separates silver islands from the QC substrate.

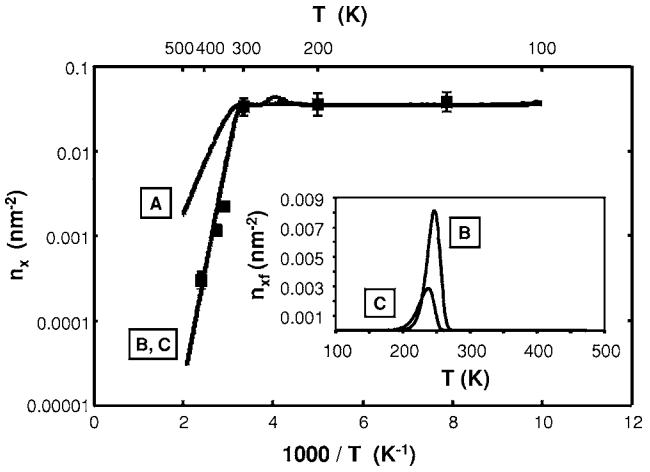

FIG. 3. Temperature dependence of the average island density, n_x, at $F=0.001$ ML/s. Solid lines show the predictions obtained from the rate equation model. The inset shows the model's prediction for the number of islands on regular terrace sites (n_{xf}) as a function of temperature.

bars at and below 300 K in Fig. 3. The error bars demarcate minimum areal island sizes of 0.5 and 1.5 nm^2 (the first corresponding roughly to single atoms[25] and the last to larger clusters of ~6 atoms).[10] The data points are obtained with a middle value of 1.0 nm^2. At and below 300 K, in Figs. 3 and 4, the statistics are very good since the data are obtained from STM images after counting thousands of islands spanning an area equal to 1×10^6 nm^2. Thus the statistical uncertainty is much smaller than the error bars shown, at these low temperatures. In contrast, at higher temperatures islands are identified unambiguously, and uncertainties are due to the limited number of islands. These uncertainties are fairly insignificant, at least on the log scale of Fig. 3.

Figure 3 shows quantitatively the temperature dependence of average island density for a deposition flux of $F=1\times10^{-3}$ ML/s. The island density is roughly constant up to 300 K, but abruptly decreases for higher temperatures. This

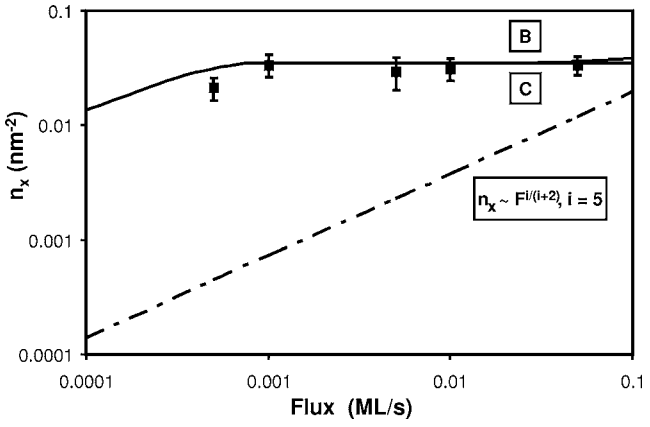

FIG. 4. Average island density, n_x, versus flux for $\theta=0.2$ ML and $T=300$ K. The solid lines depict predictions from the rate equation model for two cases, set *B* and set *C*. The expected scaling behavior for homogeneous nucleation for $i=5$ is shown by the dash-dotted line.

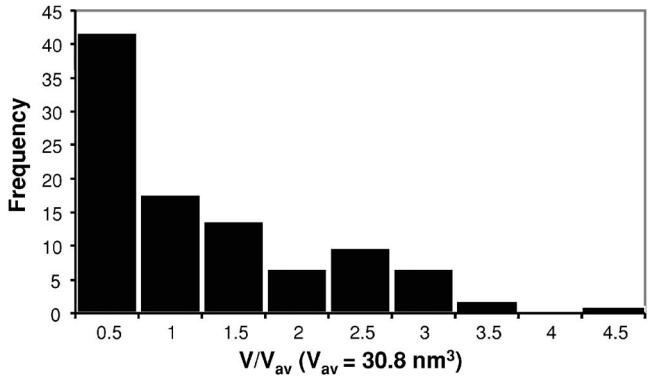

FIG. 5. Island size distribution from STM images for Ag/Al-Pd-Mn at 365 K, 0.26 ML, and $F=1\times10^{-3}$ ML/s.

is an indication that heterogeneous nucleation at trap sites dominates behavior at lower temperatures.

We also determine the influence of flux on the island density at constant temperature, 300 K. (The flux-scaling data were published previously; here, we present a reanalysis that employs the height- and size-thresholds described above.) From Fig. 4, it can be seen that the island density is insensitive to flux over the range 5×10^{-2} to 1×10^{-3} ML/s (although there may be a slight drop-off at lowest flux). An independence of island density on deposition flux is also consistent with heterogeneous nucleation at specific trap sites on the surface.

Further analysis of the STM data yields the island size distribution (ISD). Results for 300 K were presented previously, although there was considerable ambiguity in determining the true ISD as it was combined with the distribution of higher substrate protrusions.[19] Figure 5 shows new results from analysis of 365 K data. The total number of islands is about 100, so the statistics are somewhat limited (and histogram bins are necessarily chosen to be quite broad). One could measure island size either in terms of lateral area, or in terms of the total number of atoms (i.e., in terms of volume). The latter is somewhat more generic. The two approaches are equivalent for the single layer islands at lower T, but not when there is a mixture of multilayer islands of different heights as at higher T. The 365 K data reveal a monotonically decreasing ISD when size is measured as number of atoms. Such a monotonic decrease contrasts the monomodal shape of the distribution typical for homoepitaxial or heteroepitaxial growth.[26] This type of ISD could reflect unusually persistent island nucleation, and/or a diminution of growth rate with coverage.[27] Plausibly, for this system, island growth is inhibited with increasing size (a feature not incorporated into our simple rate equation analysis—see following sections) due to the fivefold symmetry of the substrate.

As an aside, we note that if the ISD at 365 K is determined by taking size as lateral area, it is instead monomodal, reflecting the feature that the largest islands are not single layer, but tend to have heights of two to four layers in this experiment.[23]

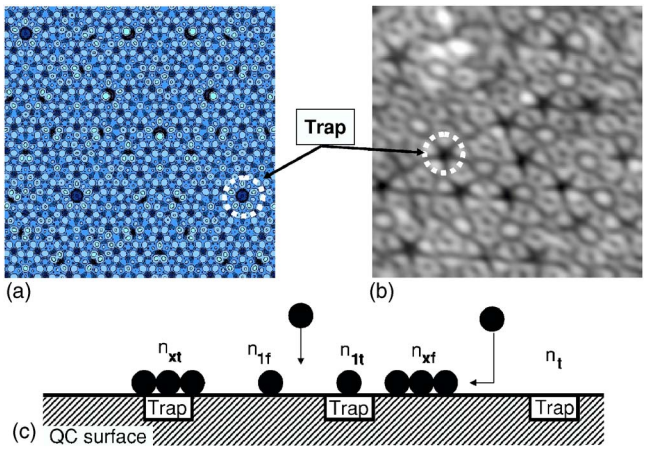

FIG. 6. (Color online) (a) Potential energy surface (8.6 $\times 8.6\text{nm}^2$) for Ag on *i*-Al-Pd-Mn QC. Darker shades indicate stronger interactions. (b) 8.6×8.6 nm^2 STM image of clean fivefold surface of *i*-Al-Pd-Mn QC (+0.97 V, 0.47 nA). One of the traps is marked both on the STM image and on the PES. (c) Model for nucleation at "trap" sites. n_{1t} is the density of trapped single adatoms; n_t is the density of traps, n_{1f} is the density of free single adatoms, n_{xf} is the density of critical clusters formed on terraces, and n_{xt} is the density of trapped stable clusters.

IV. DEVELOPMENT OF THE MODEL FOR NUCLEATION AND GROWTH OF ISLANDS

A. Potential energy surface

In developing a model for formation of Ag islands on fivefold Al-Pd-Mn surfaces, it is valuable first to have a qualitative picture of the potential energy surface (PES) describing the binding energy of Ag as a function of lateral position on this substrate. In previous work,[28] we did this for Al adatoms, and here we extend the analysis to Ag adatoms. [Other authors have recently used LJ parameters to generate the PES of various adsorbates on quasicrystals, successfully explaining experimental structures of equilibrated Al monolayers and noble gas monolayers.[16,29,30] Our work differs in that it focuses on the kinetics of formation of localized structure.] In our previous work, we identified a subset of physically-reasonable fivefold terminations of the Boudard model for bulk Al-Pd-Mn structure. We adopt one such termination here. We use pairwise-additive Lennard-Jones (LJ) potentials to describe the interaction of Ag with the substrate atoms. Parameters for the LJ potentials are chosen to recover diffusion barriers and adsorption site heights for several benchmark systems consisting of Ag on single crystal Al and Pd substrates.[31] With these interactions, we determine the binding energy of Ag as a function of lateral position while keeping substrate atoms frozen (apart from a contraction of the top layer spacings, as guided by experiment).[3,32–38]

A portion of this PES is shown in Fig. 6(a). One can identify three regions of strong bonding, each with local fivefold symmetry, in the upper left, lower left, and lower right areas of the figure. One of these is labeled "trap site." Five other regions of strong bonding, where the local fivefold symmetry is broken, are apparent in the upper middle and right portion of the figure. In our previous study of Al binding on the related *i*-Al-Cu-Fe surface, these same regions provided the strongest bonding, the former being referred to as starfish (SF) sites and the latter as incomplete starfish (ISF) sites. In addition, there is a significant number of a third type of localized strong binding site.

Corresponding features in an STM image of the fivefold Al-Pd-Mn surface are shown in Fig. 6(b). Here, we identify the SF sites with the "dark stars" often resolved in STM images of these surfaces. Experiments have proven that the dark stars are the adsorption sites of Al starfish on *i*-Al-Cu-Fe.[6,10] The SF and ISF sites, and equivalently the dark star sites, are strong candidates for the trap sites that are manifest so clearly in the experimental data of Figs. 3 and 4.

In a complete analysis of the PES, we have identified all local minima or binding sites, which include a large number of shallower binding sites in addition to the above-mentioned deep sites. Analysis of $\sim$600 sites in a 10×10 nm^2 region of the model[39] finds 0.5% of sites are SF, 1% are ISF, 4.5% are other localized deep sites, and 94% are shallow sites. The average separation between adjacent minima, regardless of depth, is $\sim$0.4 nm. We will use this value as the typical nearest-neighbor separation between adatoms in the modeling that follows.

Utilizing the above information, we can provide the following overview of the deposition process (cf. Refs. 17 and 28): Ag atoms are deposited primarily at shallow adsorption sites, and hop between such adjacent sites; occasionally they reach strong bonding "trap" sites where they remain longer and are more likely to become incorporated into stable Ag islands. (We emphasize that these trap sites are intrinsic to the surface quasicrystalline structure, and are not defects.) In principle, aggregation into islands on regions of the terrace associated with shallow sites is also possible. In our previous modeling of Al deposition on Al-Cu-Fe and Al-Pd-Mn, six atom clusters forming at SF sites (and also smaller clusters forming at ISF sites) were stabilized more effectively than clusters at non-(I)SF sites, since neighboring Al adatoms could readily reduce their separation below the typical value of $\sim$0.4 nm noted above to maximize Al-Al adatom bonding. This stabilization was not so readily achieved at other terrace sites since the large adatom separation of $\sim$0.4 nm is not compatible with strong Al-Al bonding. We adopt this feature—namely, different adatom interaction strengths at different types of nucleation sites—in the Ag modeling below.

B. Rate equation analysis

Rate equations are developed for a model of competitive island formation at trap sites and on terraces, similar to the ones in the literature for nucleation of metal clusters on oxide surfaces with defects.[40] Figure 6(c) shows a schematic of the model. The model parameters describing the system are as follows: the trap density (n_t); the trap energy ($E_t>0$) reflecting the additional binding at trap sites; the critical nucleus size (i) above which islands are stable (and for which we allow different values i_t for islands at traps, and i_f on trap-free terrace regions); the effective diffusion barrier ($E_d>0$), which describes diffusion between heterogeneous

weaker-binding adsorption sites; and the pairwise-additive nearest-neighbor adatom binding energy ($E_b > 0$). We allow E_b to take different values at traps (E_{bt}) than on the "free" parts of the terraces (E_{bf}), and set $E_{bf}=RE_{bt}$ with $R \leqslant 1$ for reasons discussed above. The effective hop rate between neighboring sites on terraces is given by $h=\nu e^{-E_d/(kT)}$ where $\nu=10^{13}$ s^{-1}. The trap density, n_t, is determined experimentally from the plateau value in Fig. 3.

Key variables to be determined by integration of the rate equations are the density of isolated adatoms, n_1 (which is the sum of contributions from traps, n_{1t}, and from "free" terrace regions, n_{1f}) and the density of stable islands, n_x (which also is a sum of contributions from traps, n_{xt}, and terraces, n_{xf}). In this model, stable clusters are regarded as immobile. We adjust values of the model parameters described above until the predicted total island density, n_x, matches experimental behavior.

We assume that a quasiequilibrium is established between the adatom densities at the traps (n_{1t}) and on the free terrace regions (n_{1f}). Accounting for the feature that adatoms are bound more strongly at traps by an amount E_t and that stable islands at traps (with density n_{xt}) block the occupation of those traps by adatoms, this quasiequilibrium assumption yields the relation (cf. Ref. 40)

$$\frac{n_{1t}}{n_t - n_{xt}} \approx \frac{n_{1f}e^{E_t/(kT)}}{1 + n_{1f}e^{E_t/(kT)}}, \tag{1}$$

where we assume that $n_{1f} \ll 1$. The rate equations for densities of stable islands are determined by the nucleation rates

$$\frac{dn_{xt}}{dt} = K_{nuct} \propto hn_{1f}n_{it} \tag{2}$$

and

$$\frac{dn_{xf}}{dt} = K_{nucf} \propto hn_{1f}n_{if}, \tag{3}$$

where n_{if} (n_{it}) is the density of critical clusters of i atoms on free terrace (trap) sites which are stabilized by addition of one further adatom. In determining these densities, we also adopt a quasiequilibrium Walton relation $n_{if} \approx e^{E_{if}/(kT)}(n_{1f})^{i_f}$ and $n_{it} \approx e^{E_{it}/(kT)}n_{1t}(n_{1f})^{i_t-1}$. Here, $E_i=m_iE_b$ denotes the binding energy for critical clusters, which is determined by adding the appropriate number, m_i, of bond energies, with relevant values of i and E_b for islands at traps or on terraces. The aggregation rates $K_{aggf} \propto h(n_{1f})n_{xf}$ and $K_{aggt} \propto h(n_{1f})n_{xt}$ also appear in the rate equation for the adatom density

$$\frac{dn_{1f}}{dt} \approx F - K_{aggf} - K_{aggt} - (i_f + 1)K_{nucf} - (i_t)K_{nuct}. \tag{4}$$

The constants of proportionality (not shown) in the expressions for nucleation rates and aggregation rates are the capture numbers for critical and stable clusters, respectively. These are always of order unity, and are set equal to unity in the following analysis. We also note that these rate equations are numerically stiff, so a natural rescaling[41] is applied before numerical integration in order to facilitate integration.

TABLE I. Parameters for best fits of the rate equation model to the experimental data.

Parameter set	A	B	C
i_t	1	5	5
i_f	1	5	11
E_d (eV)	0.18	0.66	0.66
E_t (eV)	0.60	0.50	0.50
E_{bt} (eV)	—	0.090	0.090
$R=E_{bf}/E_{bt}$	—	0.10	0.20

In general, the value of m_i depends upon the assumed cluster geometry. The two cluster sizes that will be most useful in the modeling will contain 5 and 11 atoms, for which we count $m_i=7$ and 16, respectively.

C. Model limitations and simplifications

A significant potential limitation of the rate equation analysis is the assumption of a quasiequilibrium between the population of isolated adatoms at trap sites and free terrace sites, and between the population of atoms and critical clusters (i.e., the Walton relation). This assumption is expected to be valid at high temperatures, but less so at low temperatures, where slow diffusion is expected to inhibit equilibration. A second simplification is the fact that the model uses averages or effective values for certain quantities instead of distributions. An example is the assumption of a single value of E_{bf} for atoms in clusters on the free terrace sites. On the real surface, there is a distribution of separations between adsorption sites, and also of the binding energy at those sites. [Again, see Fig. 6(a).] This means that interactions between adatoms probably vary as well. A third assumption is that bond energies, E_b, are pairwise additive within the Ag clusters. Because of these limitations, we do not regard the model as quantitatively reliable. We do regard it as useful, however, for showing major trends and providing physical insight into the relative importance of the various processes in fitting the experimental data.

V. MODELING RESULTS

First, let us consider the simplest case, where $i_t=i_f=1$ (Ag adatom pairs form stable nuclei) and thus E_b is not relevant. Such a model has only two adjustable parameters: E_t and E_d. In this case, Fig. 3 shows that the model can reproduce average island density in the low temperature regime when E_d and E_t are 0.18 and 0.60 eV, respectively. (We denote this set of parameters as set A, and summarize it in Table I.) While the model reproduces the low-temperature plateau, it fails to produce a sufficiently rapid decrease in island density above 300 K with these parameters.

Next, we allow $i_t=i_f>1$, with E_b fixed at a single nonzero value, i.e., $E_{bf}=E_{bt}$ so $R=E_{bf}/E_{bt}=1$. In this case, the model fails to fit the plateau in island density below 300 K. The reason is that, for a single binding energy and single critical size, there is no difference between the formation of stable

clusters at free terrace sites and at trap sites. The vastly higher density of the free terrace sites favors nucleation there. Indeed, depending on the adjustable parameters below 300 K the number of islands on free terrace sites is 5 to 20 times larger than at trap sites, since the latter are limited by n_t. (Changing n_t within the limits of experimental uncertainty does not help.) In our model, this problem cannot be avoided by allowing the two critical sizes to take different values. This is true at least for $2<i_f<20$ and $2<i_t<5$. (We regard these two ranges as having physically-reasonable limits.) This shows that introducing a larger critical size at free sites does not provide sufficient bias against nucleation at those sites.

In order to fit the entire range of data, we find it necessary to allow E_{bt} and E_{bf} to take independent values, i.e., to use R, their ratio, as an adjustable parameter. As mentioned in Sec. IV, values of $R<1$ have some physical justification from the potential energy surface. In the rate equation model, introducing $R<1$ gives a way to strongly destabilize clusters on free terraces. In this case, the trends in the experimental data can be reasonably well captured (see Fig. 3) by choosing a single value of critical size, $i_t=i_f=5$, together with $E_{bt}=0.090$ eV, $E_d=0.66$ eV, and $R=0.10$. We denote this set of parameters as set *B*. It does much better than set *A* in matching the high-temperature data.

However, $R=0.10$ is perhaps unrealistically low. Indeed, using the LJ potentials for bulk Ag, we estimate that the ratio of the binding energies for Ag-Ag bonds at their equilibrium separation, relative to Ag-Ag bonds elongated to 0.40 nm, is 0.33. Consequently, we explore the possibility of using higher values of R, coupled with two distinct critical sizes for trap and free sites with $i_f>i_t$. Choosing a larger critical size for free terrace sites provides some bias against nucleation on free terraces, which compensates for the higher values of R. While keeping $i_t=5$, we find that experimental data can be fit well for a range of $i_f \geqslant 8$ and $R=0.15-0.20$. The best fit is obtained when $i_t=5$ and $i_f=11$, together with $E_{bt}=0.090$ eV, $E_d=0.66$ eV, and $R=0.20$. See Fig. 3. We call this set *C*. The parameters for the three best-fit models are summarized in Table I.

The inset in Fig. 3 shows the island density on free terrace sites as a function of temperature, using sets *B* and *C*. This indicates that some Ag island nucleation does occur on regular terrace sites between 200 K and 300. However, it should also be emphasized that the contribution of free sites to average island density is low compared to that of trap sites, with these parameters.

What features of the deposition process produce the particular form of $n_x(T)$ shown in Fig. 3? Insight is provided by Fig. 7. Here, the rate of nucleation at trap sites, K_{nuct}, is shown as a function of coverage, for four different values of T. The value of K_{nuct} peaks at low coverage and decays. The peak is higher and the decay is faster at low T. At 300 K or below, K_{nuct} has effectively decayed to zero by 0.2 ML, i.e., all traps are saturated by 0.2 ML. For higher T, the slower decay of K_{nuct} means that traps are not saturated by 0.2 ML, so $n_x(T)$ in Fig. 3 drops to lower values. It follows that the temperature at which n_x begins to fall in Fig. 3 would shift to higher values for higher coverages.

Finally, the flux independence of the island density at 300 K can also be fit well. The solid lines in Fig. 4 represent

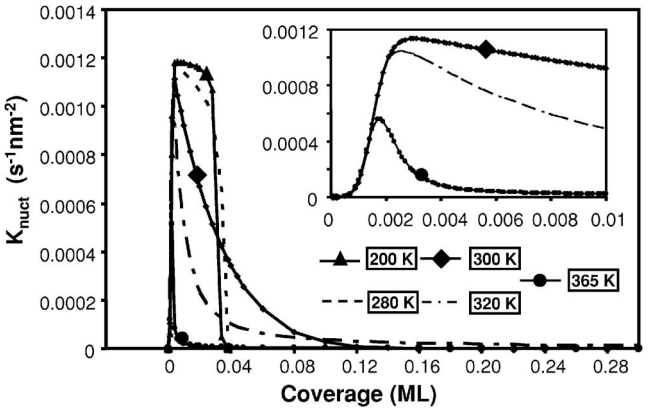

FIG. 7. The rate of nucleation at trap sites, K_{nuct}, versus coverage from the rate equation model for set *C*: $n_t=0.035$ nm^{-2}, $E_d=0.66$ eV, $E_{bt}=0.090$ eV, $m_{11}=16$, $R=0.20$, $i_f=11$, and $i_t=5$. The inset is an expanded view of the variation in K_{nuct} with coverage for the three lowest temperatures. Flux is 0.001 ML/s.

the results for sets *B* and *C*. It can be seen that with both sets of parameters, the model shows no significant variation with flux for $F>1\times10^{-3}$ ML/s. However, below this value, the model indicates that traps sites are not saturated (at this temperature and coverage), so n_x falls with decreasing flux.

Flux scaling for homogeneous nucleation of stable islands that require aggregation of $i \geqslant 1$ diffusing adatoms in the steady-state regime suggests $n_x \propto F^{i/(i+2)}$.[26,42] The dash-dotted line in Fig. 4 reflects this scaling relationship for $i=5$. Clearly this behavior does not fit experimental observations.

Using our model, we can predict n_x versus F at different deposition temperatures (Fig. 8). The model suggests that at high temperatures such as 345 K and above, the density depends on flux for the typical experimental range of fluxes shown (in contrast to behavior at 300 K and below). It would be interesting to test this prediction experimentally. The lines are slightly curved at low flux, but straighten as temperature increases. At 420 K, where the relationship is very linear, analysis of the scaling with flux indicates that $n_x \propto F^{0.66}$, rather than the relationship given above for homogeneous

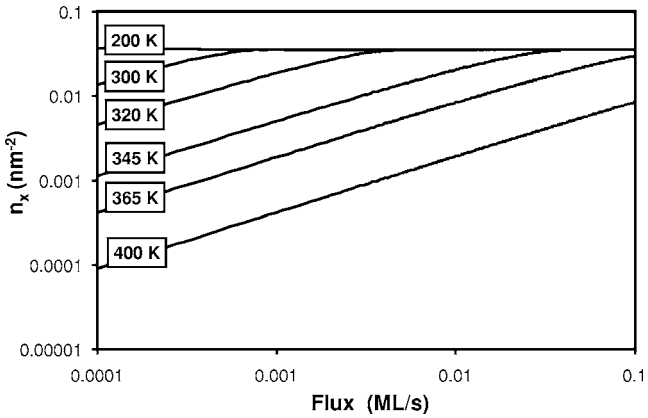

FIG. 8. Predictions for average island density, n_x, as a function of flux from the rate equation model. Parameter values correspond to set *C*: $n_t=0.035$ nm^{-2}, $E_d=0.66$ eV, $E_{bt}=0.090$ eV, $m_{11}=16$, $R=0.20$, $i_f=11$, and $i_t=5$.

nucleation with $i=5$, which would be $n_x \propto F^{5/7}=F^{0.71}$. To understand this discrepancy, we note that in this regime, n_{xf} is negligible and most traps are saturated with single adatoms, so $n_{1t} \approx n_t$. (Clusters are rare at the traps, since $n_x < n_t$ in the curves of Fig. 8.) Thus, in our rate equation analysis, one can neglect n_{xf} and simplify the equation for n_{xt} to $dn_{xt}/dt \propto (n_{1f})^{i_t}$. Then using a steady-state approximation that $F - K_{aggt} \approx 0$, it follows immediately that $n_x \propto F^{(i_t-1)/(i_t+1)}$. This yields an exponent of 2/3, consistent with the numerical results for $i_t=5$.

VI. DISCUSSION

The main result is the experimental observation that, for a typical flux, the island density is independent of temperature up to 300 K but decreases abruptly above 300 K, for a coverage of about 0.2 ML. This signifies that the island density equals the density of intrinsic surface traps up to 300 K, but falls at higher T because inhibited nucleation prevents trap saturation. The experimental flux dependence of n_x at 300 K shows no significant variation, except perhaps at lowest flux. Our interpretation is that the island density is again equal to the trap density. Limited data are also presented for the experimental island size distribution, showing a monotonic decrease at a single coverage, temperature, and flux.

A rate equation model shows that two main features must be incorporated to fit the temperature-dependent data: (1) the critical size must be significantly greater than 1, both at trap and free terrace sites; and (2) the binding energy of adatoms in the critical cluster must be significantly higher at traps than at free terrace sites. The model parameters that provide good fits for the temperature-dependence of n_x also provide good fits for the flux dependence of n_x. The model predicts significant flux dependence at $T>300$ K, where n_x is well below the trap density so that the effect of traps is reduced.

The growth dynamics that are incorporated into the model can be envisioned as follows. Adatoms are deposited on the surface and then diffuse, sometimes visiting trap sites. Additional atoms can join to form clusters, potentially either at trap sites or on terraces. However, these clusters constantly dissolve and reform if they are below the size of a stable nucleus, $i+1$. In order for nucleation to be favored at traps, the population of critical clusters of size i must be enhanced at the traps. In the case $i=1$ (when critical clusters are *single atoms*), the only important factor is the population of *single atoms* at trap sites relative to free terrace sites, which is determined in our model by the trap site energy, E_t. As i increases above 1, the binding energy of additional atoms at traps relative to that on terraces, defined in our model by R, becomes increasingly important, since this determines the stability of *other atoms* in a trap cluster relative to its free-terrace counterpart. For large critical sizes, such as those in our best solutions (sets B and C), varying E_t actually has far less effect than varying R, if E_t is above a minimum value. In fact, if $E_t \geqslant 0.40$ eV, it has no effect at all, which effectively reduces the number of variable parameters. In summary, our model shows that traps are most effective for nucleation when $i=1$ because traps have a higher population of single atoms, and also when $i>1$ because traps have a higher affinity for additional atoms.

Although the values of the best-fit parameters are not absolute because of the model limitations noted in Sec. IV, the value of 0.66 eV for E_d is somewhat high when compared with simpler crystalline surfaces. For instance, E_d is about 0.5 eV both for Ag/Al(100) and Ag/Pd(100), and E_d is much lower—about 0.1 eV—for the (111) faces.[31] In general, for single crystals, one finds that E_d increases as the surface becomes more corrugated and less close packed.[43] Thus, a relatively high value of E_d on the quasicrystal surface may be physically reasonable in light of its intrinsic roughness. It should be noted that in the rate equation analysis, E_d is an effective diffusion barrier on the free terrace. Clearly, the surface heterogeneity results in a distribution of barriers that separate adjacent minima [Fig. 6(a)]. The effective diffusion barrier reflects not only the distribution of real barrier heights but also the sampled diffusion paths. This concept of an effective barrier is standard in extensive treatments of transport in disordered systems based on homogenization or effective medium theories.[44] For our specific application, the effective barrier will be primarily controlled by the higher barriers for diffusion on the terrace.

It is interesting that the best value of i_t is 5, exactly the value expected given the stability of the 6 atom starfish clusters observed and modeled for Al on *i*-Al-Cu-Fe.[28] These clusters contained 1 atom at the center and 5 atoms at the arms, thus reflecting the local fivefold symmetry of the surface sites. Hence, the value of the critical cluster size at trap sites may be fundamentally related to the fivefold symmetry of the quasicrystalline surface.

This system bears certain similarities to transition metal clusters that form at defects on oxide[45,46] and fluoride[40] surfaces. In some of those systems, the dependence of island density on temperature has been measured,[40,45] showing a plateau and then a decline.[40,45]

For one system, Pd/MgO, these data were initially interpreted in terms of a model like the one we have used, incorporating strong trapping of adatoms at defects and subsequent island nucleation (with $i=1$) below the threshold temperature.[45] However, this model was challenged on the basis of density functional theory (DFT) calculations, which indicated that cluster diffusion, as well as monomer diffusion, should be operative, and that the surface dimer binding energy necessary to fit the data, 1.2 eV, was unreasonably high.[47,48]

We regard cluster diffusion in our system, however, as unlikely. This is because there are two primary scenarios wherein diffusion of small clusters on surfaces is expected to significantly affect growth: (1) weak bonding to the surface compared to intracluster bonding—as is the case for Pd/MgO;[48] or (2) a PES for the cluster amenable to concerted cluster motion, as for dimers in metal homoepitaxial systems where twisting or shearing motion is facile.[49] Neither scenario is operative for Ag on Al-Pd-Mn where Ag binds strongly to the surface. Inspection of the spatial distribution of adsorption sites on the surface (e.g., from the LJ PES) suggests no easy twisting pathway. In fact, intracluster binding is likely weak due to a large typical separation between neighboring adsorption sites so clusters are more likely to dissociate than diffuse. Weak intracluster binding is supported by the low value of E_b, 0.090 eV. It is also impos-

sible for clusters to migrate along with the underlying traps, as has been suggested for Au clusters on TiO_2.[46]

Our model is also qualitatively different regarding the metal-metal binding energy, which was disputed in the Pd/MgO system.[47,48] Our values of E_b are low: 0.090 eV within the traps, and less on the free terraces by a factor of R. For comparison, the Ag-Ag dimer binding energy on a Ag(100) surface is 0.22–0.26 eV.[50] The distortion from the equilibrium bond length that is imposed by the quasicrystal substrate makes the lower value of 0.090 eV plausible. There are also other differences. For instance, critical size was quite small in the rate equation analysis of the Pd/MgO system and so E_t was an important parameter. Our fits imply large critical sizes and hence virtually no dependence on E_t, for reasons discussed above. In spite of these differences, the approach that was pioneered by Haas *et al.*[45] appears to be very useful in interpreting results from the present system.

Finally, consider the possibility of place exchange between Ag and the quasicrystal substrate. We see no evidence of such a process, but if it occurred, its effect on island density would be different than our experimental observations. Typically, place exchange is an activated process, with a barrier higher than that for hopping diffusion. Growth of islands at exchange sites competes with homogeneous nucleation and growth. These two factors mean that typically, island density vs T or T^{-1} is a V-shaped (or even more complex) curve, as has been reported for Ni/Ag(100)[51] and Co/Cu(100).[52] In the case of island nucleation mediated *entirely* by place exchange, there is also a (predicted) strong dependence of island density on T, contrasting our experimental observations.[53] Hence, place exchange cannot explain our experimental observation of a plateau, followed by a decline at high T.

VII. CONCLUSIONS

A main result in this paper is that the Ag island density on the fivefold surface of icosahedral Al-Pd-Mn is independent of temperature up to 300 K, but decreases abruptly above 300 K, for a typical flux. This indicates that nucleation is dominated by trap sites at and below 300 K. This conclusion is reinforced by the experimental flux dependence of the average island density at 300 K. A rate equation model is developed, guided in part by a potential energy surface generated from Lennard-Jones potentials. For certain parameters, the model is consistent with all of the data. The optimal parameters indicate strong Ag-Ag binding at trap sites relative to free terrace sites, and large critical sizes at both types of sites. The island size distribution at 365 K is also presented, showing a broad monotonic decrease.

The data and the modeling, taken together, indicate that saturation of trap sites at low coverage is favored by low temperature and high flux. These qualitative guidelines may prove useful in searches for pseudomorphic clusters on quasicrystals at submonolayer coverages.

Note added in proof. Recently, it has come to our attention that a considerable body of work deals with heterogeneous nucleation of Co on Au, which exhibits some strong similarities to this system. See, for instance, Ref. 54.

ACKNOWLEDGMENTS

B.U., C.J.J., A.R.R., T.A.L., and P.A.T. were supported for this work by the Office of Science, Basic Energy Sciences, Materials Science Division of the U.S. Department of Energy (USDOE). V.F., K.J.S., C.G., and J.W.E. were supported by NSF Grant No. CHE-0414378. The work was performed at Ames Laboratory, which is operated for the USDOE by Iowa State University under Contract No. W-7405-Eng-82. We are thankful to Da-Jiang Liu for DFT energetics and his help during the writing of the Mathematica codes.

[1] D. Shechtman, I. Blech, D. Gratias, and J. W. Cahn, Phys. Rev. Lett. **53**, 1951 (1984).
[2] J. M. Dubois, *Useful Quasicrystals* (World Scientific, Singapore, 2005).
[3] P. A. Thiel, A. I. Goldman, and C. J. Jenks, in *Physical Properties of Quasicrystals*, edited by Z. M. Stadnik (Springer, Berlin, 1999), Vol. 126, p. 327.
[4] D. Rouxel, M. Gil-Gavatz, P. Pigeat, and B. Weber, J. Non-Cryst. Solids **351**, 802 (2005).
[5] J. M. Dubois, P. Brunet, W. Costin, and A. Merstallinger, J. Non-Cryst. Solids **334**, 475 (2004).
[6] V. Fournée and P. A. Thiel, J. Phys. D **38**, R83 (2005).
[7] R. McGrath, J. Ledieu, E. J. Cox, and R. D. Diehl, J. Phys.: Condens. Matter **14**, R119 (2002).
[8] R. McGrath, J. Ledieu, E. J. Cox, N. Ferralis, and R. D. Diehl, J. Non-Cryst. Solids **334**, 500 (2004).
[9] K. J. Franke, H. R. Sharma, W. Theis, P. Gille, P. Ebert, and K. H. Reider, Phys. Rev. Lett. **92**, 135507 (2002).
[10] T. Cai, J. Ledieu, R. McGrath, V. Fournee, T. Lograsso, A. Ross, and P. Thiel, Surf. Sci. **526**, 115 (2003).
[11] J. Ledieu, J. T. Hoeft, R. E. Reid, R. D. Diehl, T. A. Lograsso, A. R. Ross, R. McGrath, and J. A. Smerdon, Phys. Rev. Lett. **92**, 135507 (2004).
[12] J. Ledieu, J. T. Hoeft, D. E. Reid, J. A. Smerdon, R. D. Diehl, N. Ferralis, T. A. Lograsso, A. R. Ross, and R. McGrath, Phys. Rev. B **72**, 035420 (2005).
[13] M. Krajci and J. Hafner, Phys. Rev. B **71**, 184207 (2005).
[14] M. Krajci and J. Hafner, Philos. Mag. **86**, 825 (2006).
[15] V. Fournée (unpublished results).
[16] B. Bollinger, V. E. Dmitrienko, M. Erbudak, R. Luscher, H.-U. Nissen, and A. R. Kortan, Phys. Rev. B **63**, 052203 (2001).
[17] C. Ghosh, D.-J. Liu, K. J. Schnitzenbaumer, C. J. Jenks, P. A. Thiel, and J. W. Evans, Surf. Sci. **600**, 2200 (2006).
[18] P. A. Thiel and J. W. Evans, J. Phys. Chem. B **104**, 1663 (2000).
[19] V. Fournée, T. C. Cai, A. R. Ross, T. A. Lograsso, J. W. Evans, and P. A. Thiel, Phys. Rev. B **67**, 033406 (2003).

[20] B. Unal, T. A. Lograsso, A. Ross, C. J. Jenks, and P. A. Thiel, Phys. Rev. B **71**, 165411 (2005).
[21] B. Unal, T. A. Lograsso, A. R. Ross, C. J. Jenks, and P. A. Thiel, Philos. Mag. **86**, 819 (2006).
[22] WSxM 4.0 Develop 7.71 Copyright May 2005 Nanotec Electronica S. L. Available from ⟨http://www.nanotec.es⟩.
[23] V. Fournée, H. R. Sharma, M. Shimoda, A. P. Tsai, B. Unal, A. R. Ross, T. A. Lograsso, and P. A. Thiel, Phys. Rev. Lett. **95**, 155504 (2005).
[24] J. Ledieu, A. W. Munz, T. M. Parker, R. McGrath, R. D. Diehl, D. W. Delaney, and T. A. Lograsso, Surf. Sci. **433–435**, 666 (1999).
[25] M. Bott, M. Hohage, M. Morgenstern, T. Michely, and G. Comsa, Phys. Rev. Lett. **76**, 1304 (1996).
[26] J. W. Evans, P. A. Thiel, and M. C. Bartelt, Surf. Sci. Rep. **61**, 1 (2006).
[27] We present a simple deterministic theory (cf. D. Robertson and G. M. Pound, J. Cryst. Growth **19**, 269 (1973)) for the distribution, $f(s)$, of island sizes, s, at the final coverage, θ. Assume that islands are nucleated at rate $K_{nuc}(\varphi)$, and all grow at the same rate, $R_{\mathrm{agg}}(\varphi)$, dependent on the instantaneous coverage, φ. The final size of an island nucleated at coverage $\theta' < \theta$ satisfies $s(\theta') \alpha \int_{\theta'<\varphi<\theta} d\varphi R_{\mathrm{agg}}(\varphi)$, with maximum $s_{\max}=s(0)$. One then has $f(s) \alpha K_{\mathrm{nuc}}[\theta'(s)]/R_{\mathrm{agg}}[\theta'(s)]$, for $s<s_{\max}$. Here, $\theta'(s)$ is the unique nucleation coverage producing an island of size s, so $\theta'(s)$ decreases with increasing s. Thus, $K_{\mathrm{agg}}(\varphi)/R_{\mathrm{agg}}(\varphi)$ increasing with φ produces $f(s)$ decreasing with s.
[28] C. Ghosh, D.-J. Liu, C. J. Jenks, P. A. Thiel, and J. W. Evans, Philos. Mag. **86**, 831 (2006).
[29] S. Curtarolo, W. Setyawan, N. Ferralis, R. D. Diehl, and M. W. Cole, Phys. Rev. Lett. **95**, 136104 (2005).
[30] R. A. Trasca, N. Ferralis, R. D. Diehl, and M. W. Cole, J. Phys.: Condens. Matter **16**, S2911 (2004).
[31] DFT calculations by Da-Jiang Liu (unpublished) indicate that the diffusion barrier for Ag/Al(100) is 0.53 eV and for Ag/Pd(100) is 0.48 eV. Furthermore, diffusion barriers of Ag on the "smooth" (111) faces are much lower, around 0.1 eV, as is expected. Fitting the values for the (100) surfaces suggests similar strengths for the LJ Ag-Al and Al-Pd interaction parameter.
[32] C. J. Jenks and R. Bastasz, Prog. Surf. Sci. **75**, 147 (2004).
[33] C. J. Jenks, A. R. Ross, T. A. Lograsso, J. A. Whaley, and R. Bastasz, Surf. Sci. **521**, 34 (2002).
[34] M. J. Capitan, Y. Calvayrac, D. Gratias, and J. Alvarez, Physica B **283**, 79 (2000).
[35] M. Gierer, M. A. V. Hove, A. I. Goldman, Z. Shen, S.-L. Chang, P. J. Pinhero, C. J. Jenks, J. W. Anderegg, C.-M. Zhang, and P. A. Thiel, Phys. Rev. B **57**, 7628 (1998).
[36] M. Gierer, M. A. V. Hove, A. I. Goldman, Z. Shen, S.-L. Chang, C. J. Jenks, C.-M. Zhang, and P. A. Thiel, Phys. Rev. Lett. **78**, 467 (1997).
[37] A. I. Goldman and P. A. Thiel, in *Quasicrystals the State of the Art*, edited by D. P. DiVincenzo and P. J. Steinhardt (World Scientific, Singapore, 1999), Vol. 16, p. 561.
[38] J.-C. Zheng, C. H. A. Huan, A. T. S. Wee, M. A. V. Hove, C. S. Fadley, F. J. Shi, E. Rotenberg, S. R. Barman, J. J. Paggel, K. Horn, P. Ebert, and K. Urban, Phys. Rev. B **69**, 134107 (2004).
[39] Coverage is defined as the ratio of the density of adsorbed particles to the density of adsorption sites. From the PES, the density of sites corresponds to area per adsorption site of 0.167 nm^2/site.
[40] K. R. Heim, S. T. Coyle, G. G. Hembree, J. A. Venables, and M. R. Scheinfein, J. Appl. Phys. **80**, 1161 (1996).
[41] J. W. Evans and M. C. Bartelt, Langmuir **12**, 217 (1996).
[42] D. Robertson and G. M. Pound, J. Cryst. Growth **19**, 269 (1973).
[43] G. L. Kellogg, Surf. Sci. Rep. **21**, 1 (1994).
[44] L. Sanchez-Palencia and E. Zaoui, *Homogenization techniques for composite media* (Springer-Verlag, Berlin, 1985).
[45] G. Haas, A. Menck, H. Brune, J. V. Barth, J. A. Venables, and K. Kern, Phys. Rev. B **61**, 11105 (2000).
[46] E. Wahlstrom, N. Lopez, R. Schaub, P. Thostrup, A. Ronnau, C. Affrich, E. Laegsgaard, J. K. Norskov, and F. Besenbacher, Phys. Rev. Lett. **90**, 026101 (4) (2003).
[47] L. Xu, G. Henkelman, C. T. Campbell, and H. Jónsson, Phys. Rev. Lett. **95**, 146103 (2005).
[48] L. Xu, G. Henkelman, C. T. Campbell, and H. Jónsson, Surf. Sci. **600**, 1351 (2006).
[49] Z.-P. Shi, Z. Zhang, A. K. Swan, and J. F. Wendelken, Phys. Rev. Lett. **76**, 4927 (1996).
[50] P. A. Thiel and J. W. Evans, J. Phys. Chem. B **108**, 14428 (2004).
[51] J. A. Meyer and R. J. Behm, Surf. Sci. **322**, L275 (1995).
[52] R. Pentcheva, K. A. Fichthorn, M. Scheffler, T. Bernhard, R. Pfandzelter, and H. Winter, Phys. Rev. Lett. **90**, 076101 (2003).
[53] D. D. Chambliss and K. E. Johnson, Phys. Rev. B **50**, 5012 (1994).
[54] V. Repain, S. Rohat, Y. Girard, A. Tejeda, and S. Rousset, J. Phys.: Condens. Matter **18**, S17 (2006).